Phys. Status Solidi B **254**, No. 3, 1600625 (2017) / **DOI** 10.1002/pssb.201600625

Part of Special Issue on
Single-Electron Control in Solid-State Devices

physica status solidi b
www.pss-b.com
basic solid state physics

Feature Article

Electron dynamics in transport and optical measurements of self-assembled quantum dots

Annika Kurzmann*[,1], Benjamin Merkel[1], Bastian Marquardt[1], Andreas Beckel[1], Arne Ludwig[2], Andreas D. Wieck[2], Axel Lorke[1], and Martin Geller[1]

[1] Fakultät für Physik and CENIDE, Universität Duisburg-Essen, Lotharstraße 1, Duisburg 47048, Germany
[2] Chair of Applied Solid State Physics, Ruhr-Universität Bochum, Universitätsstraße 150, Bochum 44780, Germany

Received 19 September 2016, revised 5 December 2016, accepted 6 December 2016
Published online 6 January 2017

Keywords Auger recombination, electron tunneling, optics, quantum dots, resonance fluorescence, transconductance spectroscopy, transport

* Corresponding author: e-mail annika.kurzmann@uni-due.de, Phone: +49-203-3792867, Fax: +49-203-3792709

The tunneling dynamics between self-assembled quantum dots (QDs) and a charge reservoir can be measured in an all-electrical or optical detection scheme. In all-electrical transconductance spectroscopy, a two-dimensional electron gas is used to probe the evolution of the many-particle states inside an ensemble of QDs from non-equilibrium to equilibrium. The optical detection scheme measures the tunneling dynamic into a single self-assembled dot. The work done and results obtained using these different measurement techniques are reviewed and compared within this article. We will show that transconductance spectroscopy is sensitive to a time-dependent density of states and enables preparation of non-equilibrium charge and spin states for future applications in quantum information processing. The optical resonance fluorescence measurements on the electron dynamics demonstrates the influence of the exciton states on the charge-carrier dynamics and enables a systematic study of the Auger recombination in self-assembled dots.

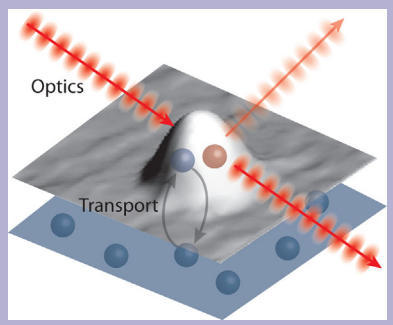

1 Introduction Quantum dots (QDs) are nanoscale objects with a confinement in all three spatial directions. They behave with their zero-dimensional density of states like "artificial atoms" and are perfectly suited for fundamental studies on atom-like quantum states [1–3] in a solid-state environment. In contrast to "real atoms," the solid-state matrix enables electrical contacting; a situation that makes QDs highly interesting for future device applications, like QD-lasers [4–6], amplifiers [7–9], photodetectors [10, 11], or memories [12–14]. More visionary applications want to use QDs as building blocks in quantum information processing [15–17]. From an application point of view again, an electrical control and detection of quantum states is here the easiest and, therefore, most desired operation for future devices – for instance an electrical read-out of an individual electron spin via spin-to-charge conversion in lithographically defined dots [18, 19]. These QDs are fabricated in a top-down approach, where local oxidation or definition of electrical gates on top of a two-dimensional electron gas produces the dot.

Another way to fabricate a three-dimensional confinement is self-assembly [20–22], for instance, by crystal growth of indium arsenide (InAs) on top of a gallium arsenide (GaAs) substrate, forming small islands with typical dimensions of a lateral size of 15–30 nm and a height of 3–8 nm. They exhibit a strong confinement for higher operation temperatures above $T = 4$ K and can be addressed by both, optical (due to their large optical dipol moment) and electrical methods. These self-assembled QDs [23, 24], like an atom, show energy quantization, direct and indirect (exchange) Coulomb

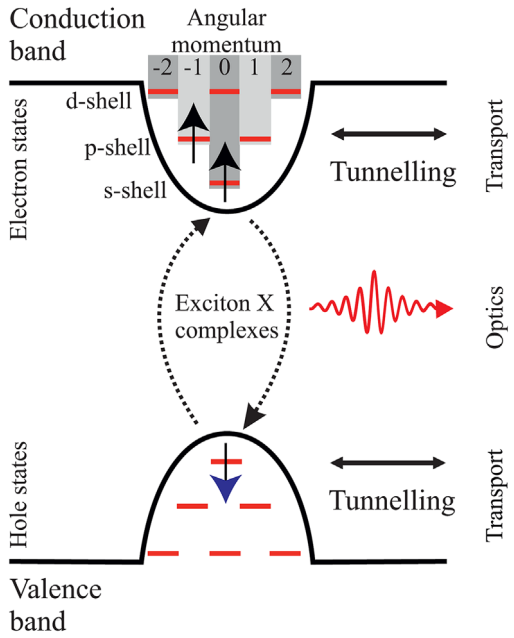

Figure 1 A schematic representation of the band structure and the energy-level scheme of a self-assembled InAs/GaAs quantum dot. In a simple picture, the dot can be described as a two-dimensional harmonic oscillator for the electron and hole states, where the s-shell is two-fold, the p-shell is four-fold, and the d-shell is six-fold degenerated.

interaction as well as angular momentum and spin-dependent optical [25–32], and electrical properties [33–36]. Moreover, recent discoveries of nuclear spin manipulation [37, 38] and decoupling from these nuclear spins [39] make self-assembled dots highly attractive for quantum applications where long spin coherence is needed.

Schematically depicted is the band structure of such a zero-dimensional, self-assembled quantum dot in Fig. 1. Depending on the semiconductor material used for the dot and the matrix, the QD has confined states for the electrons and holes in the conduction and valence band, respectively. The dot in Fig. 1 is a so-called type-I band alignment (as for InAs in a GaAs matrix), where confined electron and hole states are present in the conduction and valence band, respectively. Epitaxially grown QDs with their small height in comparison to the lateral size can be – in a very simple model – treated as two-dimensional harmonic oscillators [40]. Such a 2D harmonic oscillator has shells that are energetically separated by the quantization energy (of the order of tens of meV). These shells are called (like in atomic physics) s-, p-, and d-shell, depending on the quantum number l of the orbital angular momentum. The s-shell has a value of $l = 0$ for this quantum number and is two-fold spin degenerate, while the p-shell has two values for the quantum number $l = -1, 1$ and the d-shell has $l = -2, 0, 2$, see Fig. 1.

In capacitance–voltage [34, 41] or transport spectroscopy [42–45], the electron or hole states are measured independently with their Coulomb and exchange interaction. The electron–hole interaction is absent in such electrical measurements (for an exception, see Labud et al. [36]), where the QD has to be coupled to a charge reservoir. This reservoir provides the charge carriers, and can be used for electrical contacting and for the read-out in transconductance spectroscopy. The electron–hole interaction and recombination is in addition present in optical experiments on self-assembled quantum dots. Single photons can be absorbed and emitted in different experimental schemes, like photoluminescence [46, 47], μ-photoluminescence [48–51], differential transmission [52–54], and resonance fluorescence [55–58].

This article will review transconductance transport spectroscopy on ensembles of InAs/GaAs QDs as well as the electron dynamics into single dots studied by an optical detection that uses resonance fluorescence (RF). In transconductance spectroscopy, the many-particle ground and excited (spin) states can be prepared and detected in an all-electrical measurement scheme. In addition, the tunneling dynamics into these states are measured directly on time scales ranging from microseconds up to seconds, depending on the device geometry. The method is scalable to a single-dot level, however, this goal has not been achieved yet. Optical detection of single-electron tunneling into a single self-assembled quantum dot is reviewed in the second part of this article. With this method, the influence of the optical excitation on the tunneling dynamics and the Auger recombination can be studied in detail.

2 Electrical transconductance spectroscopy

In the following section, we will review the progress in electrical transconductance spectroscopy on an ensemble of self-assembled InAs/GaAs quantum dots. A two-dimensional electron gas (2DEG) is, on the one hand, used as a charge reservoir to inject electrons precisely into different dot states. On the other hand, the 2DEG is a very sensitive detector for time-resolved measurements of the electron tunneling, the density of states, and charge state of the dots. For comparison, this measurement technique has many similarities with the read-out process in a flash memory [14, 59].

2.1 Experimental setup and method

The experimental method of time-resolved conductance spectroscopy relies on the Coulomb interaction between the confined electrons in the dots and the two-dimensional electron gas [42, 43]. As mentioned, the 2DEG is the charge reservoir and a sensitive detector to detect the tunneling dynamics into and out of the many-particle charge and spin states [60]. Charge carriers (electrons or holes) confined within the dot lead to a reduction of the charge-carrier density in the 2DEG [44]. Simplified, every electron in the dot depletes one electron in the 2DEG. The conductivity in the electron gas is reduced and this reduction can be measured time-resolved with a time resolution that is mainly limited by the experimental setup (parasitic RC constant) and the tunneling time of the charge carrier through the tunneling barrier [61, 62]. The influence of the charged dots as Coulomb scatters can be neglected [63].

The samples discussed here were grown by molecular beam epitaxy (MBE) and processed into a "high electron

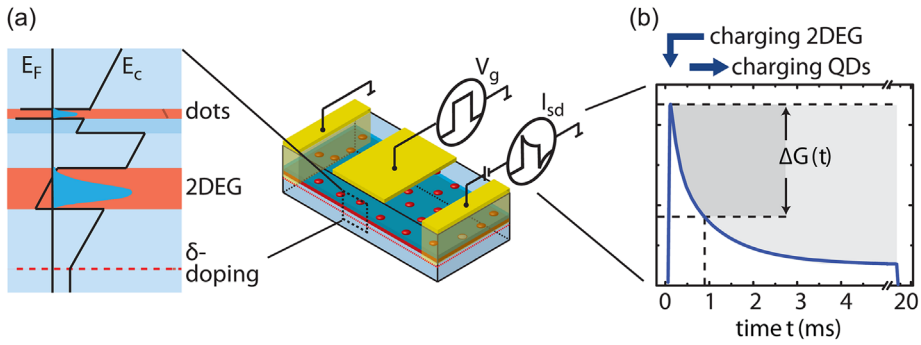

Figure 2 Schematic representation of the transconductance spectroscopy measurement principle. The InAs quantum dots are embedded in a GaAs matrix and separated by a tunneling barrier from the two-dimensional electron gas. Together with souce, drain, and gate contacts, this structure forms a "high mobility electron transistor." (a) Schematics of the conduction band profile with 2DEG and the layer of self-assembled quantum dots. The tunneling barrier is adjustable to control the average tunneling time of the electrons into the dot states. (b) After applying an electrical pulse to the gate ΔV_g, the electrical currrent $\Delta I_{sd}(t)$ is measured time-resolved. The fast increase in the current at $t = 0$ originates from charging the two-dimensional electron gas with additional electrons, while the slower decrease for $t > 0$ is due to electron tunneling into the dot states.

mobility transistor" (HEMT) structure having a source, drain and gate contact; as schematically depicted on the right-hand side of Fig. 2a. The QDs are separated from the two-dimensional electron gas by a thick tunneling barrier (10 nm $Al_{0.34}Ga_{0.66}As$ and 20 nm GaAs) that results in charge-carrier tunneling times of the order of milliseconds for large QDs. The QDs have a resonance energy of an electron–hole transition in the s-shell of about 1 eV, which equals a wavelength of 1240 nm. The left-hand side shows a schematic picture of the conduction band, where an applied gate voltage can tune the energy of the quantum dot states with respect to the Fermi level in the 2DEG, that is, by a defined gate voltage V_g the dots can be charged or discharge with electrons from the reservoir. The current through the two-dimensional electron gas is measured simultaneously while pulses are applied to the gate with an amplitude of ΔV_g. The change in the current of the 2DEG ΔI_{sd} can be measured time-resolved and is directly related to the tunneling events.

2.2 Many-particle quantum dot ground states

The electrical transconductance spectroscopy can be used to prepare and measure the many-particle ground and excited states in an ensemble of QDs. The spectrum of the ground states with their many-particle Coulomb interaction will be discussed in this section, while the excited states are reviewed afterwards in Section 2.3.

Figure 2b shows the time-resolved current through the 2DEG after the gate voltage is abruptly changed, so that the Fermi level in the 2DEG is energetically above the states of the p-shell in the dots. The fast increase in the current at $t = 0$ results from charging the electron gas and increasing the conductivity with a time constant that is limited by the *RC* constant. After this short time span, the QD states are now in a non-equilibrium situation with the electrons in the 2DEG. As a consequence, tunneling from the 2DEG to the dot states takes place and the current decreases again on a time scale of the average electron tunneling time. This can be observed as transient ΔI_{sd} with a time constant in the order of milliseconds in Fig. 2b.

Measuring such transients for different gate voltages and *fixed pulse amplitude* makes it possible to evaluate the many-particle ground states in equilibrium, shown in Fig. 3b. The pulse amplitude is fixed in this example to $\Delta V = 40$ mV. The gate voltage V_g is scanned from $V_g = -1$ V (empty QDs) up to 0.5 V (completely filled QDs). The *y*-axis shows the transient amplitude ΔI_{sd} for a situation where the QD–2DEG system has reached equilibrium (the difference in current for $t = 0$ and 20 ms). This transport measurement acts like a

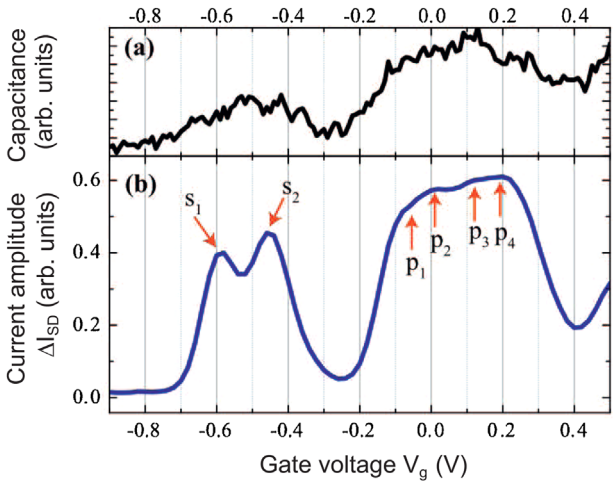

Figure 3 (a) Capacitance–voltage (*C*–*V*) spectrum of an InAs quantum dot sample with an average tunneling time of ≈ 1 ms between the 2DEG and the QD-layer. (b) The amplitude of the change in current in equilibrium ΔI_{sd} versus the applied gate voltage. Six individual peaks are visible that are caused by electron tunneling from the many-particle ground states into the two-dimensional electron gas.

"time-resolved capacitance spectroscopy," that is, the amplitude of the transient corresponds to the absolute value of the current and the time constant is related to the phase shift between the applied voltage and current in an ac capacitance measurement [33]. A comparison with a capacitance–voltage measurement in Fig. 3a shows these similarities, however, the transport spectroscopy in Fig. 3b exhibits a much higher spectral resolution.

Six individual peaks are visible in Fig. 3b. These are the quantum states of the two-dimensional harmonic oscillator up to the four-fold degenerated p-shell. The d-shell is not visible. However, the degeneracy is lifted due to the Coulomb-interaction between the electrons [33, 64].

2.3 Many-particle excited quantum dot states

Changing slightly the pulse sequence enables us to observe excited states and the relaxation dynamics from a non-equilibrium to an equilibrium situation, described in the following. An initial gate voltage V_{ini} controls the initial charge state. A negative gate voltage of $V_{\mathrm{ini}} = -1.0\,\mathrm{V}$ initially depletes the QDs completely so that all QD states are empty in the equilibrium situation at the beginning of the experiment.

What follows after the initial bias V_{ini} is again an abrupt change of the gate voltage to the probe bias V_{g}. This creates again a non-equilibrium situation between the chemical potential in the dots and the chemical potential in the 2DEG. When the chemical potential in the 2DEG is in resonance with an excited QD state, electrons can tunnel into the dots and the corresponding source–drain current I_{sd} will decrease simultaneously as described before. Keeping the initialization bias V_{ini} constant and scanning the probe bias V_{g} over the entire range from empty dots to fully charged dots yields transients of the conductance source–drain current I_{sd}, analogously to the transients shown in Fig. 3b. Please note the difference between the near-equilibrium measurement in Section 2.2 and the non-equilibrium measurement described here: In the near-equilibrium transport measurement, the initial gate voltage is changed during the measurement, while the pulse amplitude is fixed. In the non-equilibrium measurement; the initial gate voltage is fixed, while the final gate voltage (V_g in Fig. 4) and, hence, the pulse amplitude, is changed during the measurement. Moreover, in the near-equilibrium measurement, the absolute amplitude of the transient is taken as the signal, while in the non-equilibrium spectrum the first derivative of the amplitude is evaluated.

Taking the first derivative of the source–drain current amplitude I_{sd} with respect to V_{g} for a certain time t results in a spectrum, which is proportional to a time-dependent density of states [65]. Figure 4 shows a three-dimensional plot of the density of states for a transient time t between $t = 0.5\,\mathrm{ms}$ and 14 ms. We begin with the explanation for the longest time constant of 14 ms. The average tunneling time between the 2DEG and the s- and p-states is in the order of $\tau_{\mathrm{s}} = 6\,\mathrm{ms}$ and $\tau_{\mathrm{p}} = 1\,\mathrm{ms}$, respectively [42]. Setting the probe bias in resonance with a QD state and waiting 14 ms will charge the QD states to an equilibrium situation between the

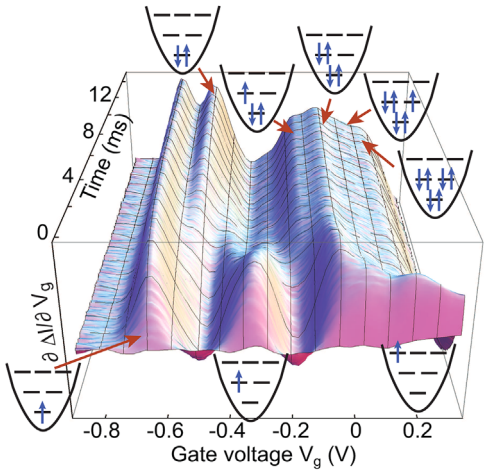

Figure 4 Time evolution of the first derivative of the source–drain current (proportional to the density of states) versus gate voltage $\partial\Delta I_{\mathrm{sd}}/\partial V_{\mathrm{g}}$. For $t = 0.5\,\mathrm{ms}$ the density of states depicts a non-equilibrium QD-hydrogen spectrum with one electron in the s-shell (at $V_g = -0.7\,\mathrm{V}$), one electron in the p-shell (at $V_{\mathrm{g}} = -0.3\,\mathrm{V}$) and one in the d-shell (at $V_{\mathrm{g}} = 0.2\,\mathrm{V}$). In a time duration of about 14 ms, the system QD–2DEG relaxes into equilibrium and the spectrum equals the equilibrium transport spectrum in Fig. 3b.

chemical potential in the 2DEG and the QDs. The s-states can also be filled via the p-states, as the electron relaxation time between theses states is in the range of picoseconds [66, 67]. Therefore, it is an almost steady-state measurement of the quantum capacitance that shows the well-known signature of the $s_{1,2}$ and p_{1-4} states as in Fig. 3b.

The fastest time window that can be evaluated by the above-discussed method is 0.5 ms. The setup is limited here to a time resolution just below 0.3 ms due to the RC time constant of the used device. The short response time, compared to the tunneling times makes it possible to ensure measuring the ground and also the excited charge states of an ensemble of completely empty QDs in a non-equilibrium situation. The presented all-electrical experiment shows the excited states of an artificial QD-hydrogen at short time delays in Fig. 4, hence, also the pure quantization energy E_0 in a self-assembled QD without any Coulomb interaction (schematically depicted as states with one electron in the s-, p-, and d-shell, respectively). In near-equilibrium measurements (like C–V spectroscopy), the electron–electron interaction (i.e., Coulomb repulsion and exchange energy) always needs to be taken into account [40]. Using the lever arm argument ($\Delta E = \lambda^{-1} e \Delta V_C$ [33, 68] with the lever arm $\lambda = 6.03$ and the elementary charge e), we can determine the quantization energy E_0 between the ground state (s-shell) and the first excited state (p-shell) to be ~50 meV. Even the second excited d-orbital can be monitored in the charging spectrum. However, the broad shoulder between 0 and 0.2 V indicates that at high gate voltages even after a very short time delay of 0.5 ms the QDs are already at least partially charged; due to tunneling into excited states and a subsequent relaxation.

Excited many-particle spin states of QD-helium and QD-lithium can also be observed by setting the initial gate voltage to different values. This is not shown here, see Marquardt et al. [60] for further information. Excited states can be prepared in an all-electrical measurement scheme using electrical transconductance spectroscopy, however, at the moment the measurement is limited to an ensemble of QDs, as the device processing has not achieved single-dot resolution yet.

3 Electron dynamics in an optical detection scheme In the following section, we will review the progress in an optical detection scheme, where the tunneling events of single electrons into a single self-assembled QD can be monitored [69–71]. The sample was also grown by molecular beam epitaxy (MBE) and processed into a Schottky-diode structure with a transparent 5 nm NiCr gate [3]. The QDs are separated from a highly n-doped back contact by a tunneling barrier (10 nm $Al_{0.34}Ga_{0.66}As$ and 20 nm GaAs) that results in electron-tunneling times of the order of μs for smaller QDs. The QDs have a resonance energy of an electron–hole transition in the s-shell of about 1.3 eV, which equals a wavelength of 954 nm. The back contact is used as a charge reservoir to prepare the QD with single-charge resolution [72, 73] the optical detection scheme is used to detect the QD charging state and to determine the tunneling rates. The transparent gate is used for the optical access to the quantum dot, while an applied voltage between the gate and back contact controls the charge state, the tunneling process, and the excitonic transition energies via the quantum confined Stark effect.

3.1 Resonance fluorescence The optical detection is carried out via the resonance fluorescence (RF) [74, 75] on a single self-assembled InAs quantum dot [55–57]. In the resonance fluorescence measurement, the QD is excited resonantly with a tunable laser directly on the excitonic transition, that is, the laser energy equals the transition energy, as schematically depicted in Fig. 5a. The sample is mounted in a bath cryostat at liquid helium temperature with an optical inset. The optical part of the setup is depicted in Fig. 5b. The exciton (X) or trion (X^-) transition are excited resonantly by a linearly polarized and frequency stabilized laser with a tunable wavelength between 910 and 980 nm. Ten percent of the laser light is guided to the sample by a 90:10 beam splitter. The laser beam is focused with an objective lens having an NA of 0.68. This results in an average diameter of the laser spot of about 1 μm and single-dot resolution is achieved. The emission of the QD is collected behind a polarizer, which is polarized orthogonally to the excitation laser and suppresses the laser light by a factor of 10^7. This suppression is the main experimental challenge to detect single QD photons on a strong laser background. The QD resonance fluorescence is detected by an avalanche photodiode (APD) having a time resolution of about 200 ps. A solid immersion lens (SIL) is mounted on top of the sample that improves the collection efficiency by a factor of four.

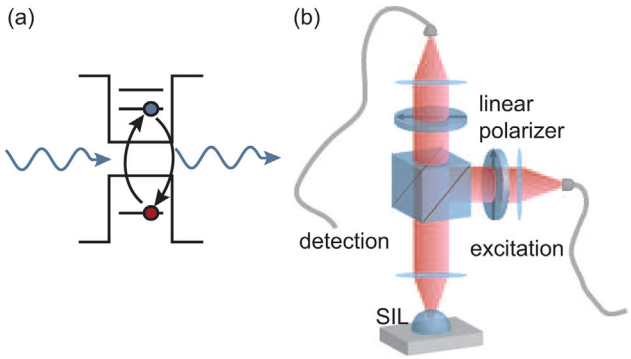

Figure 5 (a) Schematic picture of the excitation of the exciton transition in resonance fluorescence. The laser light drives the transition resonantly. (b) The optical part of the experimental set-up. The laser light is guided through a single-mode fiber, a linear polarizer, and a 90/10 beam splitter onto the sample. An objective lens with an NA of 0.68 and a solid immersion lens (SIL) onto the sample. The resonantly scattered light passes the same beam splitter again and is fed into the detection fiber after a second linear polarizer that is cross-polarized to the first one. The cross-polarization of the two polarizers suppresses the laser background in the detection arm by a factor of 10^7.

The excitonic transition in a QD can be viewed as a two-level system with the empty dot as the ground state and the bound electron–hole pair as the excited state. The interaction between a two-level system and a resonant electromagnetic wave can be calculated and the occupation probability for the upper state in a two-level system is given by [55, 76]:

$$n = \frac{1}{2}\frac{\Omega^2 T_1/T_2}{\Delta\omega^2 + 1/T_2^2 + \Omega^2 T_1/T_2}, \tag{1}$$

where T_1 is the spontaneous emission time, T_2 is the dephasing time, Ω is the Rabi frequency, and $\Delta\omega$ is the detuning between the frequency of the QD and the laser. As the number of photons emitted from the QD is proportional to the occupation in the upper level n, this equation describes the resonance fluorescence signal, which depends via the Rabi frequency $\Omega^2 \propto P$ also on the laser power P. This relation is needed later in this review. The laser power dependence of the RF intensity of the trion transition is shown in Fig. 6d. The RF intensity can be calculated by $I = I_0 n$ at a constant detuning $\Delta\omega = 0$ and is fitted to the measurements. A saturation of the RF intensity is observed for high laser excitation power. In saturation, the average occupation is $n = 0.5$ (the QD is occupied with an exciton half of the time) and the exciton recombination rate equals the absorption rate.

The RF signals of an exciton and trion are shown in Fig. 6a in a 2D-scan for different laser frequencies and gate voltages. The applied gate voltage induces the quantum-confined Stark effect [77] that shifts the resonance frequencies of the dot. The exciton transition is observed for gate voltages between −0.2 and 0.26 V, while at a gate voltage of 0.26 V, an electron tunnels into the QD, the exciton transition is quenched, and the trion is observed at lower energies (due

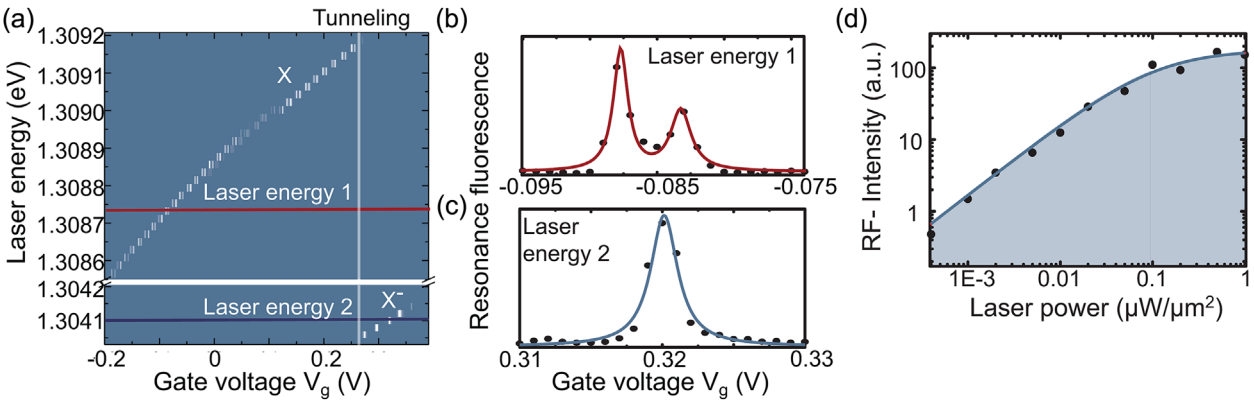

Figure 6 Resonance fluorescence (RF) of a single self-assembled InAs quantum dot. (a) Two-dimensional RF scan of the exciton and the trion transition for different laser energies and gate voltages. The exciton transition is visible in the gate voltage range between $V_g = -0.2$ V and 0.26 V. At $V_g = 0.26$ V an electron tunnels into the dot from the reservoir and the trion transition can be observed at lower energies. (b) A line-cut at a constant laser energy of 1.30874 eV for the exciton transition with its two fine-structure split bright exciton lines. (c) Another line-cut for the trion transition at a laser energy of 1.3041 eV. (d) RF intensity of the trion transition for different laser excitation powers.

to the Coulomb interaction). The RF signals of the exciton and trion transition are shown in Fig. 6b and c independently for a fixed laser frequency. In Fig. 6b, the exciton transition is observed with the two bright states, separated by the fine-structure splitting [78, 79], whereas in Fig. 6c the trion transition exhibits only one pronounced maximum.

3.2 Time-resolved observation of single electron tunneling into a single dot The resonance fluorescence can be used to determine the electron-tunneling rate in an n-shot time-resolved measurement [70]. The measurement principle works as follows: A voltage pulse is applied to the top-gate contact to charge and discharge the QD with one additional electron while simultaneously the fluorescence of the same dot is measured with a time resolution of 10 ns. The resonant excitation of the exciton transition is switched off if an electron tunnels into the dot; analogously the trion transition is switched off, when the electron tunnels out again. Every QD transition can be used for the optical detection of electron-tunneling events as the many-particle interaction in the quantum dot shifts the transitions out of resonance with the laser.

In more detail, the electrical pulse consists of two voltage settings V_1 and V_g ($V_1 < V_g$). For instance, the first gate voltage V_1 is chosen so that the QD is uncharged and the exciton transition is out of resonance with the laser frequency. Hence, no RF signal is observed. This voltage is constant during the entire measurement. The second pulse voltage V_g shifts the QD levels via the quantum-confined Stark effect so that the excitonic transition becomes in resonance with the laser energy: Just after the pulse an RF signal is observed, however, the QD is now in a non-equilibrium situation with the charge reservoir in the back contact. The Fermi level in the contact is energetically higher than the lowest level in the s-shell and tunneling into the dot occurs. This tunneling is observed by averaging over many voltage pulse cycles (an "n-shot measurement") and an exponential decay in the RF signal is observed, see Fig. 7. The additional electron stored in the dot shifts the optical transition out of resonance with the laser: The RF signal vanishes.

An example of such a pulsed optical resonance fluorescence measurement is shown in Fig. 7 for three different voltages V_g. For $V_g = 0.255$ V, the RF signal is nearly constant. A comparison with the static RF measurement in Fig. 7a shows that the exciton transition X can be excited and no tunneling into the QD is possible (as schematically depicted in Fig. 7d, left) and the RF signal of the exciton transition is nearly constant. The small decrease in the RF intensity has its origin in tunneling of electrons into the exciton state, which will be discussed in more detail in Section 3.3.

At a gate voltage of $V_g = 0.267$ V, an exponential decay of the RF signal of the X is observed that saturates at a factor of about 40% of the maximum normalized RF amplitude. In an n-shot measurement, this steady-state value of the amplitude describes the probability (here 60%) for finding the electron inside the dot after the Fermi levels in the dot and the reservoir have equilibrated. At $V_g = 0.275$ V, the exciton transition quenches completely. Here, an electron tunnels with a probability of 100% into the s-shell of the dot, see also schematic picture in Fig. 7d, right.

Taking the equilibrium amplitude of the transients in Fig. 7a at $t = 40$ ms for the different gate biases yields the Fermi distribution in the back contact (see Fig. 7c) with a temperature of 4.2 K, in perfect agreement with the expected value for liquid helium.

3.3 Electron tunneling into the exciton state A main difference from the electrical measurements in Section 2 is the optical generation of electron–hole pairs (excitons) inside the dot. The following consequences are induced by the exciton in the dot: (i) The electron from the reservoir can also tunnel into a dot containing an additional excition. As a result, the tunneling rate will be influenced by the exciton and can, hence, (ii) also be tuned by the optical

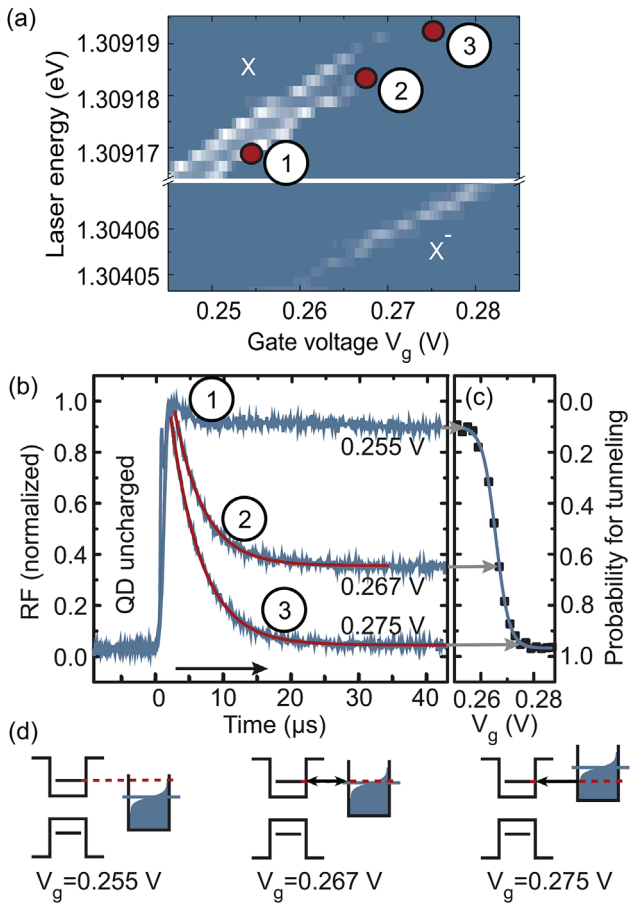

Figure 7 (a) A zoom-in to the resonance fluorescence scan of Fig. 6a with red dots marking the gate voltages that are used in the time-resolved measurements. (b) Time-resolved RF of the exciton transition during an applied gate voltage pulse. The tunneling of an electron into the QD is observed as a quenching of the intensity in an n-shot measurement. (c) Equilibrium amplitude of the time-resolved measurements for different gate voltages that resembles the Fermi-distribution of the back contact. (d) Schematic pictures of the electron tunneling between the charge reservoirs.

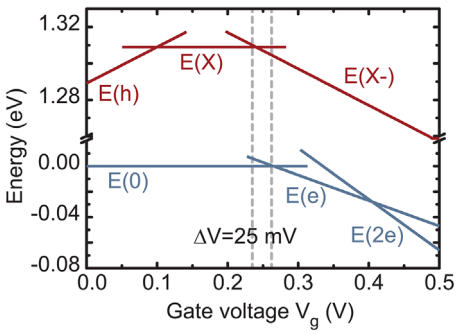

Figure 8 Energies of the different many-particle states inside the QD versus gate voltage. The calculation shows that tunneling into the excitonic state becomes energetically allowed 0.25 mV below the gate voltage for electron tunneling into an empty dot.

excitation [71]. In this subsection, we will focus on the first issue (i) in more detail by taking a closer look into the different energies that have to be taken into account to understand the tunneling dynamics. The possibility to tune the tunneling rate (the second issue (ii)) will be discussed in Section 3.4 later.

The gate voltages where tunneling into the different excitonic states is possible can be calculated using a simple model that is described in Seidl et al. [73, 80]. The energies of the different charge states are given by the Coulomb interaction and the electrostatic potential. These energies can be calculated by using the recombination energy of the exciton and trion and the gate voltage for electron tunneling of the first and second electron into the dot. The blue curve in Fig. 8 shows the energies and transition voltages from an empty QD with energy $E(0)$ to a doubly negatively charged system $E(2e)$. At a gate voltage of $V_g = 0.265$ V, one electron can tunnel into the empty QD (see Fig. 6a), visible as intersection between the energy of the empty and the singly charged dot. With this intersection the confinement potential of the dot ($E_C = 172$ meV) is determined. The intersection between the energy of the singly and doubly charged QD gives the Coulomb interaction between the electrons of $E_{ee} = 28$ meV.

Furthermore, the electron–hole Coulomb interaction can be calculated to $E^{eh} = 33$ meV and the bandgap is given by $E_g = 1342$ meV. With this values the energies of the different excitonic states are calculated and plotted versus the gate voltage in Fig. 8. The intersection between the energy of the exciton and the trion indicates the gate voltages, where tunneling into the excitonic state is possible. This gate voltage is 25 mV smaller than the gate voltage for tunneling into the empty dot. The smaller gate voltage explains the small decrease in the amplitude of the RF signal in Fig. 7b at $V_G = 0.255$ V. The electron can tunnel already into the exciton state where no tunneling into the empty dot is possible.

3.4 Optical tuning of the tunneling rate After calculating the different energies and gate voltages for the electron-tunneling events in the previous subsection, we want to concentrate now on the expected tunneling rate with and without the presence of an additional exciton. The time-resolved RF transients can be calculated by solving a master equation approach [81, 82]. This is a common method to model a system with discrete states and to describe the time-dependent occupation probabilities.

In our calculation, we distinguish between a fluorescent and a non-fluorescent state. The fluorescent state includes two sub-states: the empty QD (0) and the QD filled with one exciton (X). The non-fluorescent state includes also two substates: A dot that is occupied with one electron (e) and the negatively charged trion (X^-). If the QD is in resonance with the laser, it is possible to excite an exciton X with the absorption rate γ_{abs}. The exciton X can recombine with the recombination rate γ_{rec} and the probability for finding an exciton in the dot is given by: $n = \gamma_{abs}/(\gamma_{abs} + \gamma_{rec})$. Furthermore, an electron tunnels into the empty dot with the tunneling rate γ_{In} and out of the dot with the tunneling rate

γ_{Out}. Tunneling into the excitonic state takes place with the tunneling rate $\gamma_{\text{In}}^{\text{X}}$. The overall relaxation rate into equilibrium

$$\gamma_m = \gamma_{\text{Out}} + (1-n)\gamma_{\text{In}} + n\gamma_{\text{In}}^{\text{X}}, \tag{2}$$

is obtained [71], which is directly measured in the transients in Fig. 7. The results show the influence of the occupation probability with an exciton n on the relaxation rate γ_m, which is further described in the following.

The in- and out-tunneling rates γ_{In} and γ_{Out} can be expressed with Fermi's golden rule [83, 84]:

$$\gamma_{\text{In}} = 2\Gamma f(E), \tag{3}$$

$$\gamma_{\text{Out}} = 1\Gamma(1 - f(E)), \tag{4}$$

where Γ is the intrinsic tunneling rate and $f(E)$ the Fermi function. $\gamma_{\text{In}}^{\text{X}}$ is constant with $\gamma_{\text{In}}^{\text{X}} = 1 \cdot \Gamma_{\text{In}}^{\text{X}}$ and does not depend on the gate voltage as the Fermi distribution equals unity.

The factor of two in γ_{In} originates from the spin degeneracy of the QD states. Two spin directions are possible for tunneling of one electron into the s-shell of an empty dot (Fig. 9a), that is, $d_{\text{In}} = 2$. If the dot is occupied by one electron, the degeneracy for tunneling out is $d_{\text{Out}} = 1$ (Fig. 9c). For tunneling into the exciton state in Fig. 9b, the degeneracy would be also $d_{\text{In}} = 1$, if the exciton were a stable ground state. However, it is an excited state that decays within the radiative lifetime and the average occupation of the exciton state depends on the excitation laser power: At low power, the dot is empty most of the time, at high power, the average exciton occupation saturates at one half. In saturation, the QD is half of the time occupied with an exciton and the degeneracy for tunneling into the dot is reduced from $d_{\text{In}} = 2$ to $d_{\text{In}} = 1.5$. The tunneling is optically blocked at high laser excitation power by tuning the degeneracy.

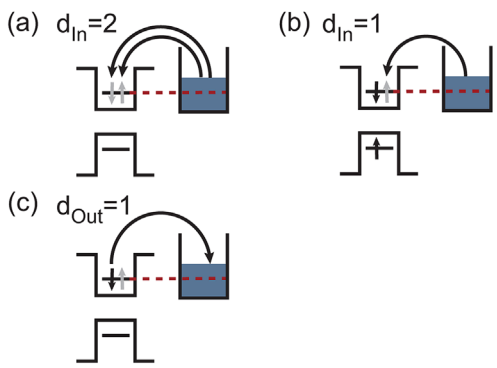

Figure 9 Schematic picture for the different spin degeneracies. For tunneling into an empty dot, the degeneracy is (a) $d_{\text{In}} = 2$, into the excitonic state (b) $d_{\text{In}} = 1$, and out of the singly charged QD (c) $d_{\text{Out}} = 1$. It shows that an optical blocking for electron tunneling into the QD is achieved when the QD is occupied by an additional exciton.

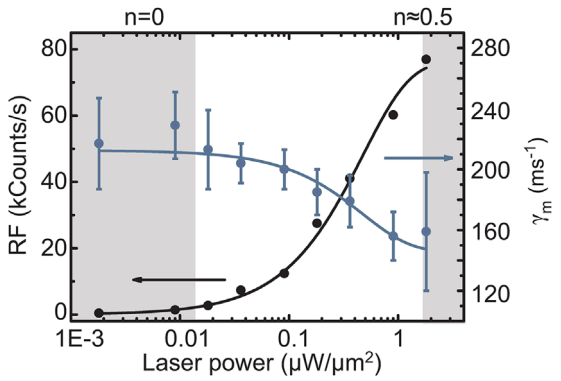

Figure 10 Relaxation rate γ_m into equilibrium for different laser excitation power. The overall relaxation rate γ_m is reduced (blue line) with increasing laser power, due to the optical blocking effect. The black line shows the exciton RF signal for increasing laser power.

The optical blocking can be observed in the time-resolved RF measurement as a decrease of the relaxation rate γ_m for increasing laser power (blue data points in Fig. 10). The laser power changes the average occupation with an exciton from $n = 0$ to $n = 0.5$, which can be observed by an increase of the RF signal, black line in Fig. 10. The optical blocking can be used to change and control the tunneling rates into a self-assembled QD by optical means on an extremely fast time scale that is in principal only limited by the Rabi frequency.

3.5 Optical excitation on the trion transition

Up to now, the optical detection was realized by resonant excitation of the exciton transition. As a consequence, the exciton line was switched off after tunneling of an electron into the dot. However, this optical detection scheme also works for all other excitonic transitions. As an example, results on the trion transition will be shown in this subsection.

For a time-resolved measurement of the trion state the QD is first charged with one electron. Then, the electron tunneling back into the charge reservoir can be observed as a decreasing RF intensity.[1] Figure 11 shows as an example, the transients for different gate voltages. For $V_{\text{g}} = 0.252$ V, the RF intensity of the trion decreases to zero at $t = 40$ ms as the QD is always uncharged in equilibrium and the trion transition is out of resonance with the laser. For increasing gate voltage, an increasing equilibrium amplitude of the RF intensity is observed, similar to the measurement before, where the Fermi distribution in the back contact directly determined the value of this amplitude.

An interesting observation can be made at a gate voltage of $V_{\text{g}} = 0.276$ V. The Fermi distribution equals unity in the back contact (see Fig. 11b, right) and the transient in Fig. 11a should be constant and exhibits no decrease in the RF intensity; in contrast to the observations made in Fig. 11a. This

[1] The laser power is decreased here to a situation were the average occupation of the dot with an exciton can be neglected.

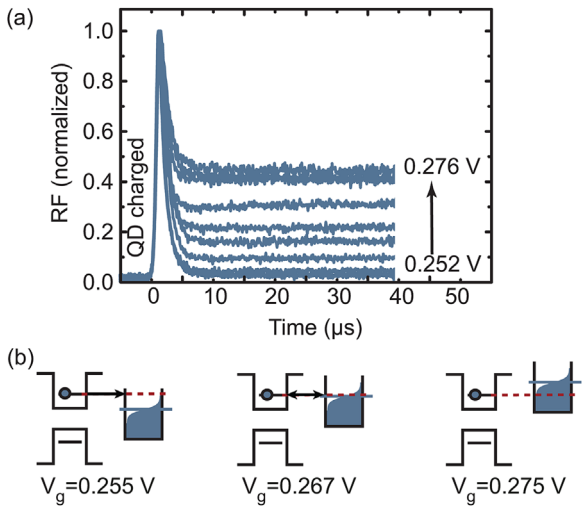

Figure 11 (a) Time-resolved RF measurement of electron tunneling on the trion transition. At $t = 0$ μs, tunneling of an electron from the s-shell of the dot into the reservoir is possible, depending on the value of the gate voltage. At $V_g = 0.252$ V the electron in the dot will tunnel with 100% probablity into the reservoir, quenching the trion transition. At $V_g = 0.276$ V, the electron should stay in the dot and a constant RF amplitude is expected. However, the decrease of the amplitude shows, that the electron is also emitted by an Auger-type recombination. (b) Schematic pictures with Fermi distribution and tunneling events for different gate voltages.

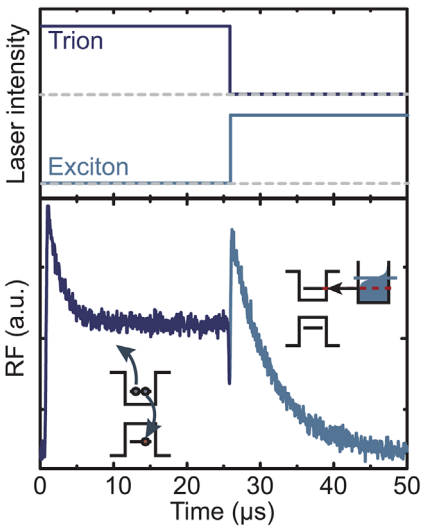

Figure 12 The Auger recombination and electron tunneling measured in a two-color excitation experiment. (a) Laser-pulse sequence for the resonant excitation of the first laser on the trion and the second laser on the exciton transition. (b) The time-resolved measurement shows the Auger recombination by laser excitation on the trion transition between $t = 0$ and 25 μs. After $t = 25$ μs, the electron tunneling into the dot is observed by laser excitation on the exciton transition.

unusual decrease of the RF amplitude at $V_g = 0.276$ V has its origin in a non-radiative Auger recombination, that will be discussed in the following section.

3.6 Auger recombination The Auger process is a non-radiative recombination process. In a quantum-confined semiconductor structure (like a quantum dot), the exciton energy is transferred to a third charge carrier. No photon is emitted and the excess charge is transferred from the dot state into the continuum of the semiconductor. For a negatively charged exciton (the negative trion) it means that the recombination energy of the exciton removes the additional electron from the dot. The dot is in its empty ground state and can no longer be excited on the trion energy.

Two lasers with two different frequencies can be used to measure the Auger recombination. The first laser (laser frequency 1) is in resonance with the trion energy and the second laser (laser frequency 2) is in resonance with the exciton energy. The resonance fluorescence of the exciton and the trion transition can now be observed at the same gate voltage, a situation that is not possible in equilibrium and works as follows: The Auger recombination discharges the QD under resonant trion excitation; leaving an empty dot for driving the exciton transition. The uncharged dot can be excited on the exciton transition until an electron tunnels from the charge reservoir into the dot with the tunneling rate γ_{In} in an n-shot measurement, see Fig. 12. For each shot, at $t = 0$ μs the QD is charged with one electron and the trion laser is switched on. This leads to an excitation of the trion transition and enables the Auger recombination. The Auger process is observed as an exponential decay of the trion RF signal. For the given experimental situation we find a decay rate of $\gamma_m = 0.77\ \mu\mathrm{s}^{-1}$. At $t = 25$ μs, the trion laser is switched off so that the Auger-recombination is no longer possible, while at the same time the exciton laser is switched on. Now, the exciton transition is in resonance with the laser and an RF signal of the exciton is observed for times $t > 25$ μs. The exciton transition is switched off by the electron tunneling into the dot. The evolution of an empty to a charged QD is observed as an exponential decay in the excitonic RF signal for $t > 25$ μs with a tunneling rate of about $\gamma_{\mathrm{In}} = 0.18\ \mu\mathrm{s}^{-1}$.

The relaxation rate was determined for different laser excitation powers in a time-resolved n-shot RF measurement, shown in Fig. 13a. Again the laser power changes the probability n for an additional exciton inside the dot (in addition to the electron). The time evolution of the normalized RF signal is nearly constant for $n = 0.003$ (low laser power), where the dot is most of the time not in the trion state. As a consequence, the Auger recombination is negligible. [2] For a probability of an exciton inside the QD of $n = 0.2$, an exponential decay of the RF signal is observed that saturates slightly below a value of 0.5. At this laser excitation power, 50% of the measurements end in a situation where the electron was removed from the QD by Auger recombination. At $n = 0.5$ (saturated

[2] Note here that the RF signal is normalized; the overall intensity for $n = 0.003$ is much smaller than for $n = 0.5$.

excitation), 80% of the RF signal quenches, indicating that the QD is empty with 80% probability under saturated excitation. This value depends on the ratio between Auger recombination γ_a and tunneling rate γ_{In},which are affected by the size of the dot (Auger rate) [85] and the tunneling barrier thickness (tunneling rate).

The relation between the tunneling rate and quenching of the trion RF signal can be determined by a rate equation model. The time evolution of the resonance fluorescence signal P is given by the differential equation

$$\dot{P}_f = \gamma_{\text{In}} P_{\text{nf}}(t) - n\gamma_a P_{\text{f}}(t), \tag{5}$$

where P_{nf} and P_{f} are the occupation probabilities for the empty dot (non-fluorescent state) and the charged trion state (fluorescent state), respectively. The average occupation of the QD with an exciton is given by n. The boundary condition $P_f(0) = 1$ is used to solve Eq. (1). We obtain

$$P_{\text{f}}(t) = \frac{\gamma_{\text{In}} + n\gamma_a e^{-\gamma_m t}}{\gamma_{\text{In}} + n\gamma_a}, \tag{6}$$

with the relaxation rate

$$\gamma_m = \gamma_{\text{In}} + n\gamma_a, \tag{7}$$

$P_f(t)$ directly reflects the measured transients in Fig. 13 with a relaxation constant γ_m given by Eq. (7) and shown in Fig. 13b. To determine the Auger recombination rate from Eq. (7), the tunneling rate $\gamma_{\text{In}} = 0.2\,\mu\text{s}^{-1}$ is needed that can be obtained with a fit of Eq. 7 to the data in Fig. 13b. An Auger recombination rate $\gamma_a = 2.3\,\mu\text{s}^{-1}$ is determined.

Using the knowledge of the Auger process in colloidal QDs [85] with an Auger rate that depends on the radius r of the dot as $r^{-6.5}$, we find an expected Auger rate of $2.8\,\mu\text{s}^{-1}$ for an estimated QD size of 20 nm. The estimated Auger recombination rate fits perfectly into the outcomes from the measurements. However, the small Auger rate in self-assembled QDs can be explained by their lateral size. The small tunneling rate for electrons into the dot from the reservoir $\gamma_{\text{In}} = 0.2\,\mu\text{s}^{-1}$ in our sample (in the same order of magnitude as the Auger rate) offers the possibility to observe the Auger recombination in self-assembled dots.

The intensity of the trion state as a ratio between tunneling rate and Auger rate for different exciton populations n is given for $t \to \infty$ in Eq. (6):

$$P_{\text{f}}(\infty) = \frac{\gamma_{\text{In}}}{\gamma_{\text{In}} + n\gamma_a}, \tag{8}$$

This equilibrium amplitude of the trion state in presence of the Auger recombination is shown in Fig. 14 for two different laser powers. At small laser excitation, the average occupation is $n = 0.01$ (red line) and for high laser excitation it is $n = 0.5$ (blue line). Clearly visible is the influence of the tunneling rate on the RF intensity of the trion. For high tunneling rates in comparison to the Auger rate ($\gamma_{\text{In}} > 10\gamma_a$), the RF intensity of the trion is not quenched, due

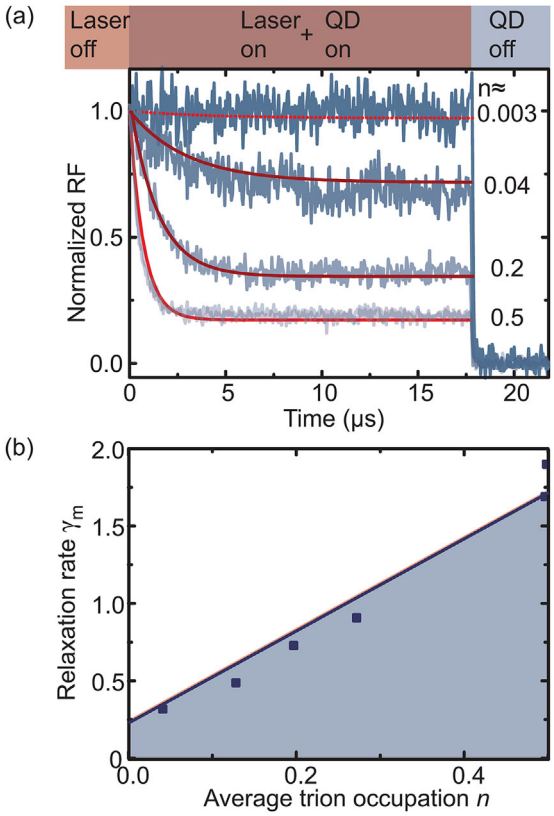

Figure 13 (a) Time-resolved resonance fluorescence on the trion transition for different laser excitation powers. The laser power changes the average occupation with a trion n up to a value of $n = 0.5$ in saturation. The laser is turned on at $t = 0$ and a quenching of the trion transition is observed with a relaxation rate γ_m. (b) The relaxation rates γ_m for different laser powers are plotted versus the probability for a electron–hole pair inside the QD.

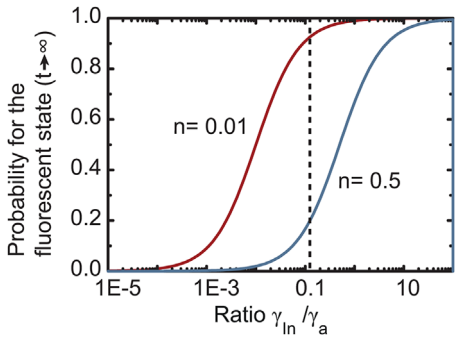

Figure 14 Probability P for a fluorescent state (photon emission from the trion transition) in equilibrium versus the ratio between tunneling rate γ_{In} and Auger recombination rate γ_a. The fluorescence of the trion transition completely quenches for a ratio of $\gamma_{\text{In}}/\gamma_a = 10^{-4}$, where the tunneling rate is much smaller than the Auger recombination rate. The vertical dashed line indicated the ratio between tunneling and Auger rate in the sample used for the measurements.

to the fast tunneling of electrons into the QD. After the Auger recombination, an electron tunnels immediately into the QD and the trion is again in resonance with the laser. For small tunneling rates ($\gamma_{\text{In}} < 10^{-4}\gamma_a$), the trion RF is completely quenched at $n = 0.5$. In this situation, the QD is empty after an Auger process (i.e., in the non-fluorescent state) and the probability to return to the fluorescent state by electron tunneling is low. For a smaller laser excitation power $n = 0.01$ in Fig. 14, the probability for an Auger process is strongly reduced, keeping the QD for the same tunneling rate with higher probability in the fluorescent state (red line).

4 Conclusions The electron dynamics in self-assembled QDs has been studied in transport and optical measurements. In transport measurements on an *ensemble* of QDs, many-particle states can be prepared and detected in an all-electrical measurement scheme. The tunneling dynamics between the dots and the reservoir is measured time-resolved, yielding a time-dependent density of states. The time-resolved measurement shows the evolution of the many-particle states from non-equilibrium intoequilibrium.

In the optical measurement, resonance fluorescence was used to detect the tunneling of a single electron into a *single* self-assembled QD. This measurement scheme leads to a deeper understanding of the tunneling processes and the influence of the QDs states' degeneracy on the tunneling rates. Furthermore, the optically excited exciton changes the overall tunneling rate into the QD and opens up the possibility of an optical manipulation of its rate. Another effect of the optical excitation on the electron dynamics is the Auger recombination, which removes an electron from the QD, when an exciton recombines.

Acknowledgements This work was supported by the DFG (Contract No. GE 2141/1-1) in the framework of the NanoSci-E+ Project No. QD2D of the European Commission and the Mercator Research Center Ruhr (MERCUR) of Stiftung Mercator, as well as Project No. QuaHL-Rep 16BQ1035 and "Hochfunktionale Speicher" (HOFUS) within the VIP program of the BMBF. We also acknowledge finantial support by the collaboration research center SFB 1242. A. Ludwig and A. D. Wieck acknowledge gratefully support of DFG-TRR160 and BMBF – Q.com-H 16KIS0109.

References

[1] S. Tarucha, D. G. Austing, T. Honda, R. J. van der Hage, and L. P. Kouwenhoven, Phys. Rev. Lett. **77**, 3613–3616 (1996).
[2] S. Tarucha, D. G. Austing, Y. Tokura, W. G. van der Wiel, and L. P. Kouwenhoven, Phys. Rev. Lett. **84**, 2485–2488 (2000).
[3] P. M. Petroff, A. Lorke, and A. Imamoglu, Phys. Today 46–52 (2001).
[4] D. Bimberg, N. Kirstaedter, N. N. Ledentsov, Z. Alferov, P. S. Kop'ev, and V. M. Ustinov, IEEE J. Sel. Top. Quantum Electron. **3**, 196–205 (1997).
[5] R. L. Sellin, C. Ribbat, M. Grundmann, N. N. Ledentsov, and D. Bimberg, Appl. Phys. Lett. **78**, 1207 (2001).
[6] C. Ribbat, R. L. Sellin, I. Kaiander, F. Hopfer, N. N. Ledentsov, D. Bimberg, A. R. Kovsh, V. M. Ustinov, A. E. Zhukov, and M. V. Maximov, Appl. Phys. Lett. **82**, 952 (2003).
[7] D. Bimberg and N. Ledentsov, J. Phys.: Condens. Matter **15**, R1063–R1076 (2003).
[8] A. J. Zilkie, J. Meier, P. W. E. Smith, M. Mojahedi, J. S. Aitchison, P. J. Poole, C. N. Allen, P. Barrios, and D. Poitras, Opt. Express **14**, 11453 (2006).
[9] J. Park, N. J. Kim, Y. D. Jang, E. G. Lee, J. M. Lee, J. S. Baek, J. H. Kim, H. S. Lee, K. J. Yee, D. Lee, S. H. Pyun, W. G. Jeong, and J. Kim, Appl. Phys. Lett. **98**, 011107 (2011).
[10] S. H. Hwang, J. C. Shin, J. D. Song, W. J. Choi, J. I. Lee, and H. Han, Microelectron. J. **36**, 203–206 (2005).
[11] P. Martyniuk and A. Rogalski, Prog. Quantum Electron. **32**, 89–120 (2008).
[12] M. Geller, A. Marent, T. Nowozin, D. Bimberg, N. Akçay, and N. Öncan, Appl. Phys. Lett. **92**, 092108 (2008).
[13] T. Nowozin, A. Marent, M. Geller, D. Bimberg, N. Akçay, and N. Öncan, Appl. Phys. Lett. **94**, 042108 (2009).
[14] T. Nowozin, A. Beckel, D. Bimberg, A. Lorke, and M. Geller, Appl. Phys. Lett. **104**, 053111 (2014).
[15] C. H. Bennett and D. P. DiVincenzo, Nature **404**, 247–255 (2000).
[16] H. J. Kimble, Nature **453**, 1023–1030 (2008).
[17] T. D. Ladd, F. Jelezko, R. Laflamme, Y. Nakamura, C. Monroe, and J. L. O'Brien, Nature **464**, 45–53 (2010).
[18] J. M. Elzerman, R. Hanson, L. H. van Willems Beveren, B. Witkamp, L. M. K. Vandersypen, and L. P. Kouwenhoven, Nature **430**, 431–435 (2004).
[19] R. Hanson, L. H. W. van Beveren, I. T. Vink, J. M. Elzerman, W. J. M. Naber, F. H. L. Koppens, L. P. Kouwenhoven, and L. M. K. Vandersypen, Phys. Rev. Lett. **94**, 196802 (2005).
[20] D. Leonard, J. Vac. Sci. Technol. B **12**, 1063 (1994).
[21] R. Nötzel, Semicond. Sci. Technol. **11**, 1365–1379 (1996).
[22] N. N. Ledentsov, V. A. Shchukin, M. Grundmann, N. Kirstaedter, J. Böhrer, O. Schmidt, D. Bimberg, V. M. Ustinov, A. Y. Egorov, A. E. Zhukov, P. S. Kop'ev, S. V. Zaitsev, N. Y. Gordeev, Z. I. Alferov, A. I. Borovkov, A. O. Kosogov, S. S. Ruvimov, P. Werner, U. Gösele, and J. Heydenreich, Phys. Rev. B **54**, 8743–8750 (1996).
[23] D. Bimberg, M. Grundmann, and N. N. Ledentsov, Quantum Dot Heterostructures (Wiley, Chichester, 2001).
[24] M. S. Skolnick and D. J. Mowbray, Annu. Rev. Mater. Res. **34**, 181–218 (2004).
[25] A. Imamoglu and Y. Yamamoto, Phys. Rev. Lett. **72**, 210–213 (1994).
[26] P. P. Paskov, P. O. Holtz, B. Monemar, J. M. Garcia, W. V. Schoenfeld, and P. M. Petroff, Phys. Rev. B **62**, 7344–7349 (2000).
[27] P. Michler, A. Imamoglu, M. Mason, P. Carson, G. Strouse, and S. Buratto, Nature **406**, 968–970 (2000).
[28] R. Rinaldi, P. V. Giugno, R. Cingolani, H. Lipsanen, M. Sopanen, J. Tulkki, and J. Ahopelto, Phys. Rev. Lett. **77**, 342–345 (1996).
[29] M. Bayer, A. Schmidt, A. Forchel, F. Faller, T. L. Reinecke, P. A. Knipp, A. A. Dremin, and V. D. Kulakovskii, Phys. Rev. Lett. **74**, 3439–3442 (1995).
[30] M. Bayer, O. Stern, P. Hawrylak, S. Fafard, and A. Forchel, Nature **405**, 923–926 (2000).

[31] A. N. Vamivakas, Y. Zhao, C. Y. Lu, and M. Atatüre, Nature Phys. **5**, 198–202 (2009).
[32] C. Matthiesen, M. Geller, C. H. H. Schulte, C. Le Gall, J. Hansom, Z. Li, M. Hugues, E. Clarke, and M. Atatüre, Nature Commun. **4**, 1600 (2013).
[33] H. Drexler, D. Leonard, W. Hansen, J. P. Kotthaus, and P. M. Petroff, Phys. Rev. Lett. **73**, 2252–2255 (1994).
[34] A. Lorke, R. J. Luyken, A. O. Govorov, J. P. Kotthaus, J. M. Garcia, and P. M. Petroff, Phys. Rev. Lett. **84**, 2223–2226 (2000).
[35] D. Reuter, P. Kailuweit, A. D. Wieck, U. Zeitler, O. Wibbelhoff, C. Meier, A. Lorke, and J. C. Maan, Phys. Rev. Lett. **94**, 026808 (2005).
[36] P. A. Labud, A. Ludwig, A. D. Wieck, G. Bester, and D. Reuter, Phys. Rev. Lett. **112**, 046803 (2014).
[37] M. Munsch, G. Wust, A. V. Kuhlmann, F. Xue, A. Ludwig, D. Reuter, A. D. Wieck, M. Poggio, and R. J. Warburton, Nature Nanotechnol. **9**, 671–675 (2014).
[38] G. Wust, M. Munsch, F. Maier, A. V. Kuhlmann, A. Ludwig, A. D. Wieck, D. Loss, M. Poggio, and R. J. Warburton, Nature Nanotechnol. **11**, 885 (2016).
[39] J. H. Prechtel, A. V. Kuhlmann, J. Houel, A. Ludwig, S. R. Valentin, A. D. Wieck, and R. J. Warburton, Nature Mater. **15**, 981–986 (2016).
[40] R. J. Warburton, B. T. Miller, C. S. Dürr, C. Bödefeld, K. Karrai, J. P. Kotthaus, G. Medeiros-Ribeiro, P. M. Petroff, and S. Huant, Phys. Rev. B **58**, 90657–16231 (1998).
[41] B. T. Miller, W. Hansen, S. Manus, R. J. Luyken, A. Lorke, J. P. Kotthaus, S. Huant, G. Medeiros-Ribeiro, and P. M. Petroff, Phys. Rev. B **56**, 6764–6769 (1997).
[42] B. Marquardt, M. Geller, A. Lorke, D. Reuter, and A. D. Wieck, Appl. Phys. Lett. **95**, 022113 (2009).
[43] B. Marquardt, M. Geller, A. Lorke, D. Reuter, and A. D. Wieck, Physica E **42**, 2598–2601 (2010).
[44] B. Marquardt, M. Geller, B. Baxevanis, D. Pfannkuche, A. D. Wieck, D. Reuter, and A. Lorke, Nature Commun. **2**, 209 (2011).
[45] D. Zhou, A. Beckel, A. Ludwig, A. D. Wieck, M. Geller, and A. Lorke, Appl. Phys. Lett. **106**, 243105 (2015).
[46] S. Raymond, S. Fafard, P. J. Poole, A. Wojs, P. Hawrylak, S. Charbonneau, D. Leonard, R. Leon, P. M. Petroff, and J. L. Merz, Phys. Rev. B **54**, 11548–11554 (1996).
[47] R. Heitz, A. Kalburge, Q. Xie, M. Grundmann, P. Chen, A. Hoffmann, A. Madhukar, and D. Bimberg, Phys. Rev. B **57**, 9050–9060 (1998).
[48] J.-Y. Marzin, Y.-M. Gerard, A. Izrael, D. Barrier, and G. Bastard, Phys. Rev. Lett. **73**, 716–719 (1994).
[49] J. C. Kim, H. Rho, L. M. Smith, H. E. Jackson, S. Lee, M. Dobrowolska, and J. K. Furdyna, Appl. Phys. Lett. **75**, 214 (1999).
[50] P. Michler, A. Kiraz, C. Becher, W. V. Schoenfeld, P. M. Petroff, L. Zhang, E. Hu, and A. Imamoglu, Science **290**, 2282–2285 (2000).
[51] E. Stock, T. Warming, I. Ostapenko, S. Rodt, A. Schliwa, J. A. Töfflinger, A. Lochmann, A. I. Toropov, S. A. Moshchenko, D. V. Dmitriev, V. A. Haisler, and D. Bimberg, Appl. Phys. Lett. **96**, 093112 (2010).
[52] K. Karrai and R. J. Warburton, Superlattices Microstruct. **33**, 311–337 (2003).
[53] B. D. Gerardot, S. Seidl, P. A. Dalgarno, R. J. Warburton, M. Kroner, K. Karrai, A. Badolato, and P. M. Petroff, Appl. Phys. Lett. **90**, 221106 (2007).
[54] A. Hogele, S. Seidl, M. Kroner, K. Karrai, R. J. Warburton, B. D. Gerardot, and P. M. Petroff, Phys. Rev. Lett. **93**, 217401 (2004).
[55] A. Muller, E. B. Flagg, P. Bianucci, X. Y. Wang, D. G. Deppe, W. Ma, J. Zhang, G. J. Salamo, M. Xiao, and C. K. Shih, Phys. Rev. Lett. **99**, 187402 (2007).
[56] R. Melet, V. Voliotis, A. Enderlin, D. Roditchev, X. L. Wang, T. Guillet, and R. Grousson, Phys. Rev. B **78** (2008).
[57] C. Matthiesen, A. N. Vamivakas, and M. Atature, Phys. Rev. Lett. **108**, 093602 (2012).
[58] A. V. Kuhlmann, J. Houel, D. Brunner, A. Ludwig, D. Reuter, A. D. Wieck, and R. J. Warburton, Rev. Sci. Instrum. **84**(7), 1–17 (2013).
[59] A. Marent, M. Geller, and D. Bimberg, Microelectron. J. **40**, 492–495 (2009).
[60] B. Marquardt, A. Beckel, A. Lorke, A. D. Wieck, D. Reuter, and M. Geller, Appl. Phys. Lett. **99**, 223510 (2011).
[61] T. Nowozin, A. Marent, G. Hönig, A. Schliwa, D. Bimberg, A. Beckel, B. Marquardt, A. Lorke, and M. Geller, Phys. Rev. B **84**, 075309 (2011).
[62] T. Nowozin, A. Marent, D. Bimberg, A. Beckel, B. Marquardt, A. Lorke, and M. Geller, Phys. Status Solidi C **9**, 243–246 (2012).
[63] A. Kurzmann, A. Beckel, A. Ludwig, A. D. Wieck, A. Lorke, and M. Geller, J. Appl. Phys. **117**, 054305 (2015).
[64] M. Fricke, A. Lorke, J. P. Kotthaus, G. Medeiros-Ribeiro, and P. M. Petroff, Europhys. Lett. **36**, 197 (1996).
[65] A. Beckel, A. Kurzmann, M. Geller, A. Ludwig, A. D. Wieck, J. König, and A. Lorke, Europhys. Lett. **106**, 47002 (2014).
[66] T. Müller, F. F. Schrey, G. Strasser, and K. Unterrainer, Appl. Phys. Lett. **83**, 3572 (2003).
[67] M. Geller, E. Stock, C. Kapteyn, R. Sellin, and D. Bimberg, Phys. Rev. B **73**, 205331 (2006).
[68] G. Medeiros-Ribeiro, D. Leonard, and P. M. Petroff, Appl. Phys. Lett. **66**, 1767 (1995).
[69] A. Kurzmann, A. Ludwig, A. D. Wieck, A. Lorke, and M. Geller, Nano Lett. **16**, 3367–3372 (2016).
[70] A. Kurzmann, A. Ludwig, A. D. Wieck, A. Lorke, and M. Geller, Appl. Phys. Lett. **108**, 263108 (2016).
[71] A. Kurzmann, B. Merkel, P. A. Labud, A. Ludwig, A. D. Wieck, A. Lorke, and M. Geller, Phys. Rev. Lett. **117**, 017401 (2016).
[72] R. J. J. Warburton, C. Schaflein, D. Haft, F. Bickel, A. Lorke, K. Karrai, J. M. M. Garcia, W. Schoenfeld, and P. M. M. Petroff, Nature **405**(6789), 926–929 (2000).
[73] S. Seidl, M. Kroner, P. Dalgarno, A. Högele, J. Smith, M. Ediger, B. Gerardot, J. Garcia, P. Petroff, K. Karrai, and R. Warburton, Phys. Rev. B **72**, 195339 (2005).
[74] M. L. Citron, H. R. Gray, C. W. Gabel, and C. R. Stroud, Phys. Rev. A **16**, 1507–1512 (1977).
[75] H. J. Kimble, M. Dagenais, and L. Mandel, Phys. Rev. Lett. **39**, 691–695 (1977).
[76] R. Loudon, The Quantum Theory of Light, 3rd edn., reprint edition, Oxford science publications (Oxford Univ. Press, Oxford, 2010).
[77] S. S. Li and J. B. Xia, J. Appl. Phys. **88**, 7171 (2000).
[78] M. Bayer, G. Ortner, O. Stern, A. Kuther, A. A. Gorbunov, A. Forchel, P. Hawrylak, S. Fafard, K. Hinzer, T. L. Reinecke, S. N. Walck, J. P. Reithmaier, F. Klopf, and F. Schäfer, Phys. Rev. B **65**, 195315 (2002).
[79] R. Seguin, A. Schliwa, S. Rodt, K. Potschke, U. W. Pohl, and D. Bimberg, Phys. Rev. Lett. **95**, 257402 (2005).

[80] P. Dalgarno, J. Smith, J. McFarlane, B. Gerardot, K. Karrai, A. Badolato, P. Petroff, and R. Warburton, Phys. Rev. B **77**, 245311 (2008).
[81] C. W. J. Beenakker, Phys. Rev. B **44**, 1646–1656 (1991).
[82] A. Beckel, A. Ludwig, A. D. Wieck, A. Lorke, and M. Geller, Phys. Rev. B **89**, 155430 (2014).
[83] P. A. M. Dirac, Proc. R. Soc. A: Math. Phys. Eng. Sci. **114**, 243–265 (1927).
[84] E. Fermi, Nuclear Physics, revised edition, reprint (University of Chicago Press, Chicago, 1974).
[85] R. Vaxenburg, A. Rodina, A. Shabaev, E. Lifshitz, and A. L. Efros, Nano Lett. **15**, 2092–2098 (2015).